

Introduction of Rotor Dynamics Using Implicit Method in LS-DYNA[®]

Liping Li
Roger Grimes

*Livermore Software Technology Corporation
7374 Las Positas Road
Livermore, CA 94551*

Abstract

Rotor dynamics is commonly used to analyze the behavior of structures ranging from jet engines and steam turbines to auto engines and computer disk drives. In such applications, the amplitude of structural vibration can become excessive when the speed of rotation approaches the system's critical speed.

This paper introduces a primary implementation of rotor dynamics in LS-DYNA and presents a validation study of this new implemented feature with exiting theoretical studies, as well as another finite element method software ANSYS. The structural vibration responses of four different models with beam, shell and solid elements, the shaft whirling orbit and Campbell diagrams are compared. It shows that the results from LS-DYNA have very good agreements with theoretical results and ANSYS simulation results. So it suggests that the LS-DYNA simulation is accurate for the cases investigated in this paper.

1. Introduction

Rotor dynamics is a specialized branch of engineering science concerned with the behavior and diagnosis of rotating structures. It is a study of vibration of rotating parts found in a wide range of equipments including engines, turbines, aircrafts, hard disk drives and more. In these applications, the critical speed - the theoretical angular velocity that excites the natural frequency of a rotating object - is of particular concern, as the resonant vibration, in which mechanical systems will oscillate excessively, can occur at such speed. It may lead to premature fatigue failure in those rotating components, as well as bearings and support structures. Besides of the critical speed, other factors, such as unbalance response, gyroscopic effects are also of interests in rotor dynamic systems.

The rotation of rigid bodies, mainly those with regular shapes, like shafts, disks and cylinders, has been well understood for several decades. However, for flexible bodies, especially those with irregular shapes, their rotational behavior requires more modern tools such as finite element method. Quite a lot studies ([1] and [2]) have presented the theoretical foundation of rotor dynamics. The finite element formulation has also been investigated by some researchers, such as J. Barlow [3].

As the critical speed, as well as unbalance response, gyroscopic effects are very important issues needed to be investigated thoroughly, we started a primary implementation of rotor dynamics in LS-DYNA. A validation study of this new implemented feature is presented with exiting theoretical studies, as well as another finite element software ANSYS. The structural vibration responses of four different models with beam, shell and solid elements, the shaft whirling orbit and Campbell diagrams are compared. It is demonstrated that the results from LS-DYNA are very similar to the theoretical results and ANSYS simulation results. So it suggests that the LS-DYNA simulation is accurate for the cases studied in this paper.

2. Implementation in LS-DYNA

Rotor dynamics is usually studied in the rotating reference frame, in which the finite element equilibrium equation can be written as:

$$[M]\{\ddot{u}\} + ([C] + [G])\{\dot{u}\} + ([K] + [K_c])\{u\} = \{F\} \quad (1)$$

where [M], [C] and [K] are the system mass, damping and stiffness matrices, respectively. [G] is the gyroscopic damping matrix. [K_c] is the softening centrifugal stiffness matrix.

A new keyword card *CONTROL_IMPLICIT_ROTATIONAL_DYNAMICS is added to LS-DYNA to study the above rotor dynamic characteristics. The parameters are listed in the following table:

*Table 1 Parameters in card *CONTROL_IMPLICIT_ROTATIONAL_DYNAMICS*

Card	1	2	3	4	5	6	7	8
Variable	pid	omega	vid	nomega				
Type	I	F	I	I				
Variable	omeg1	omeg2	omeg3	omeg4	omeg5	omeg6	omeg7	omeg8
Type	F	F	F	F	F	F	F	F

In the above table, pid is the part ID of the rotating component; omega is the rotating speed of the defined part; vid is the vector ID used to define the rotating axis vector, which is determined by the keyword *DEFINE_VECTOR. nomega is the number of rotating speeds. If it is a modal analysis, the Campbell diagram is available when nomega is a positive integer and the rotating speeds are defined by the following lines. omegi is the ith rotating speed. We can define as many rotating speeds as 80 in the current implementation. Because most rotating structures can be modeled using 1-D beam, 2-D shell and 3-D solid elements, this new rotor dynamic feature is available for these three types of elements.

3. Capabilities of Rotor Dynamics Analysis

In this section, we will use the new implemented feature in LS-DYNA to carry out three types of analysis.

3.1 Structural Vibration Analysis

Four different cases are applied for a validation study of LS-DYNA in this section. The first case is a shaft with beam element. The shaft model is shown in Figure 1, in which e is the eccentricity of the center of gravity (G) from the shaft axis center (S); y is the lateral distance of 'S' from 'O', which is also called deflection. When the shaft is rotating, it may well go into transverse oscillation. The deflection y can be calculated by the following equation:

$$y = \frac{\omega^2 e}{\omega_n^2 \left(1 - \frac{\omega^2}{\omega_n^2}\right)} = \frac{e}{\left(\frac{\omega_n}{\omega}\right)^2 - 1} \quad (2),$$

where ω is the rotating speed of the disk along the shaft axis, ω_n is the critical speed of the shaft. In order to verify LS-DYNA's capability to calculate the deflection y , a shaft model with beam element is created. Then the shaft deflection with respect to the rotating speed is plotted in Figure 2, in which the blue curve is the deflection simulated by LS-DYNA and the red curve is the theoretical results obtained from Eqn. (2). The two methods gave almost the same results. So we can say LS-DYNA is able to calculate the deflection for the shaft model.

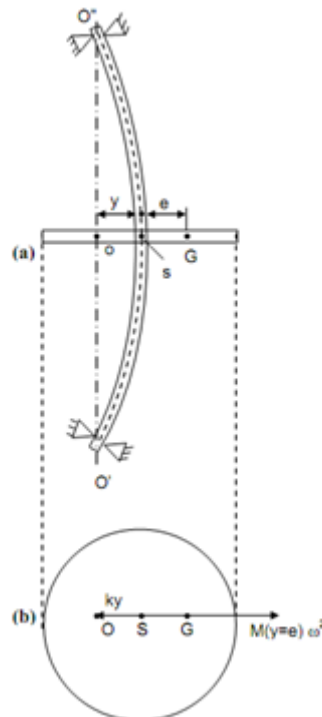


Figure 1 A shaft model

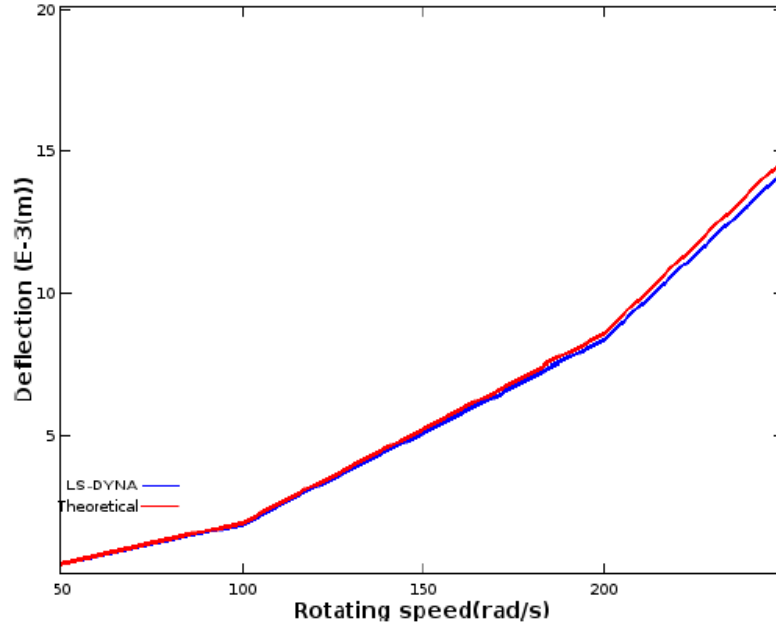


Figure 2 The shaft deflection comparison between LS-DYNA and theoretical results with $\omega_n = 523.86$ and $e = 0.05$

The second case is a disk with shell element shown in Figure 3. The disk rotates with z-axis. The dimension of the inner radius is 10 mm and the outer radius is 32.5 mm. In rotating coordinate system, the inner radius has fixed boundary condition. When the disk rotates, its in-plane displacement will increase in the radius direction due to the centrifugal force. The theoretical in-plane displacement can be calculated by the following equation [4]:

$$u(r) = c_1 r + \frac{c_2}{r} - \frac{\rho h \Omega^2}{8D^o} r^3 \tag{3}$$

whre

$$c_1 = \frac{\rho h \Omega^2}{8D^o} \left(\frac{r_o^4(3+\nu) + r_i^4(1-\nu)}{r_o^2(1+\nu) - r_i^2(1-\nu)} \right), \quad c_2 = -\frac{\rho h \Omega^2}{8D^o} r_o^2 r_i^2 \left(\frac{r_o^2(3+\nu) - r_i^2(1+\nu)}{r_o^2(1+\nu) - r_i^2(1-\nu)} \right), \quad D^o = \frac{Eh}{(1-\nu^2)}$$

ρ is the disk density; h is the thickness, Ω is the rotating speed, r_o is the outer radius, r_i is the inner radius, E is the young's modulus and ν is the Poisson's ratio.

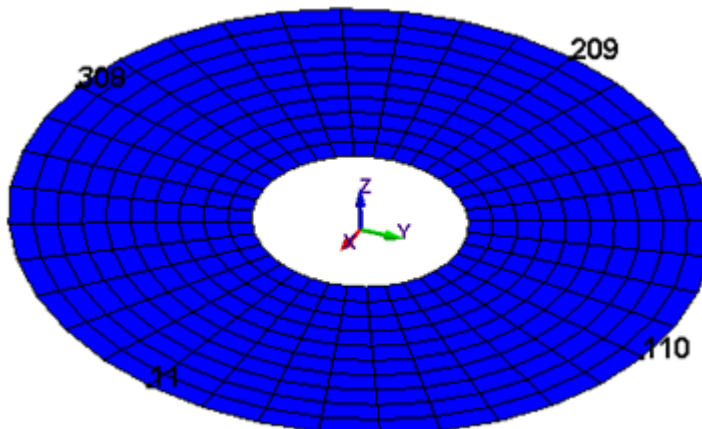


Figure 3 A disk model with shell element

The theoretical displacement at the disk’s outer radius (32.5 mm) is around 5.4×10^{-5} mm from the above equation. The following Figure 4 plots the x displacement of node 11, which locates on the x-axis. It shows that the converged displacement is around 5.53×10^{-5} mm, which is very close to the theoretical displacement 5.4×10^{-5} mm. It indicates that LS-DYNA can accurately calculate the disk’s in-plane displacement.

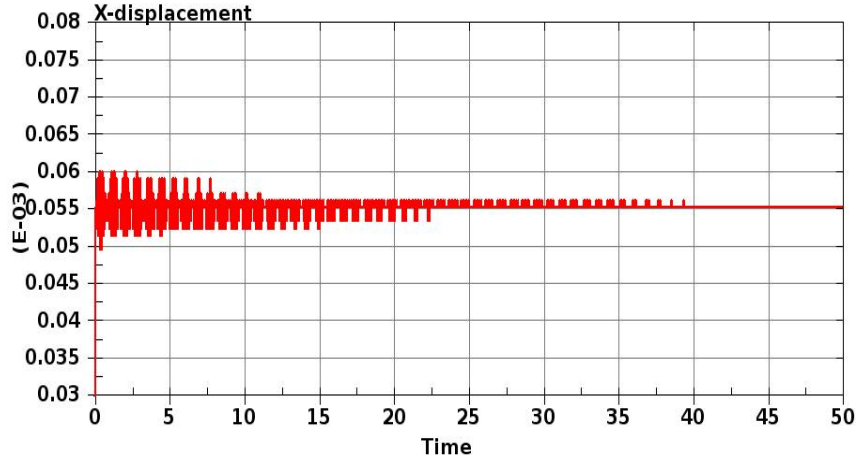


Figure 4 The x displacement of node 11 (on the outer radius)

To verify the vibration response for a model with solid element, we created a hollow cylinder model as shown in Figure 5(1). The inner and outer radiuses of the cylinder are 10 and 32.5 mm, respectively. The theoretical in-plane displacement is still applicable in this case, so the displacement on the outer radius should also be 5.4×10^{-5} mm. Figure 5(2) plots the displacement of the four nodes on the outer radius. The converged displacements are all around 5.36×10^{-5} mm, which is very close to the theoretical result.

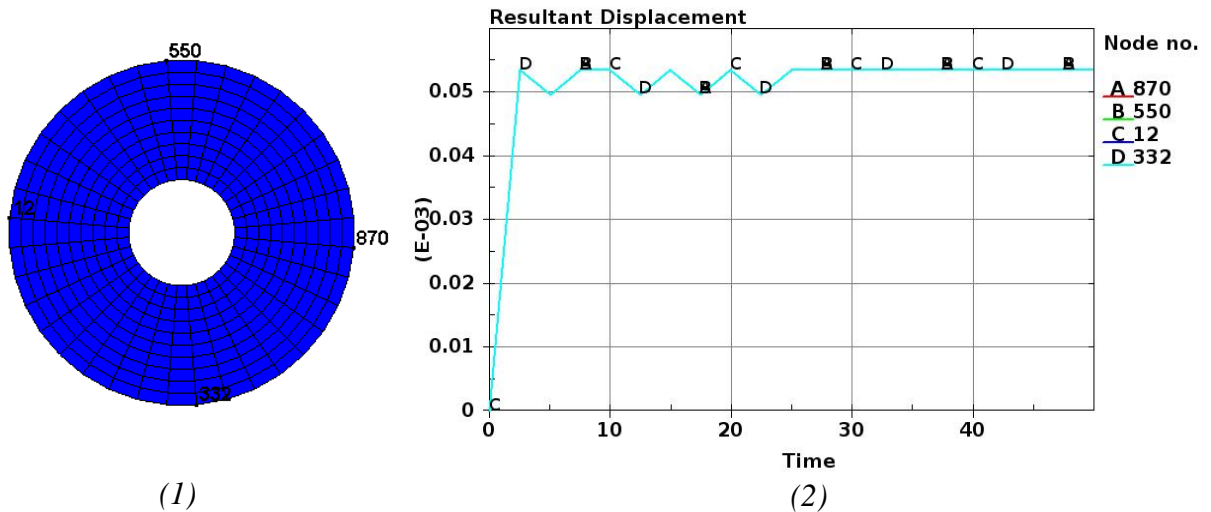


Figure 5 (1) A hollow cylinder model with solid element; (2) the displacements of the nodes on the outer radius

The last model is a quarter of a disk rotating with y-axis shown in Figure 6. As there is no theoretical displacement formula for this model, we compared the x and y displacements for node 11 and 143 using LS-DYNA and ANSYS. The unit used in LS-DYNA is ‘g, mm and ms’, while it is ‘kg, m and s’ in ANSYS. Figure 7 compares the x displacement history of node 11 for

LS-DYNA (Figure 7(1)) and ANSYS (Figure 7(2)). The x-axis is the simulation time, which is 50 ms for both simulations. The converged x displacement got from LS-DYNA is $1.9e-5$ mm, while it is $1.8e-8$ m from ANSYS (they use different units). The displacement difference is very small for the two simulations. Figure 8(1) and 8(2) show the y displacements of node 11 obtained from LS-DYNA and ANSYS. The converged values of Figure 8(1) and 8(2) are $-4.2e-4$ mm and $-4.3e-7$ m, respectively. The difference is negligible. Figure 9 and 10 compare the x and y displacements of node 143 for the two software. From Figure 9, the converged displacement for LS-DYNA is $5.24e-4$ mm and it is $5.31e-7$ m for ANSYS. The results are almost the same. From Figure 10, the converged displacement for LS-DYNA is $8.01e-5$ mm and it is $8.36e-8$ m for ANSYS. The difference is less than 5%. From the above comparison of LS-DYNA and ANSYS results, we can say that LS-DYNA gives almost the same results as ANSYS for the disk model shown in Figure 6.

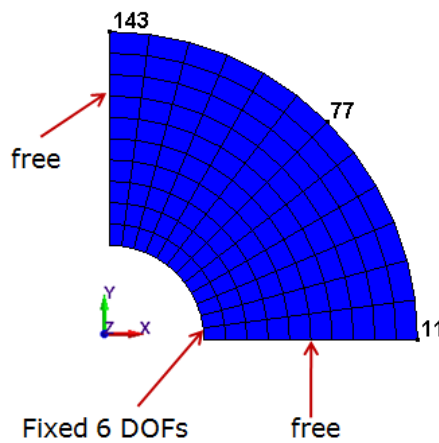


Figure 6 A quarter of disk model with the shell element

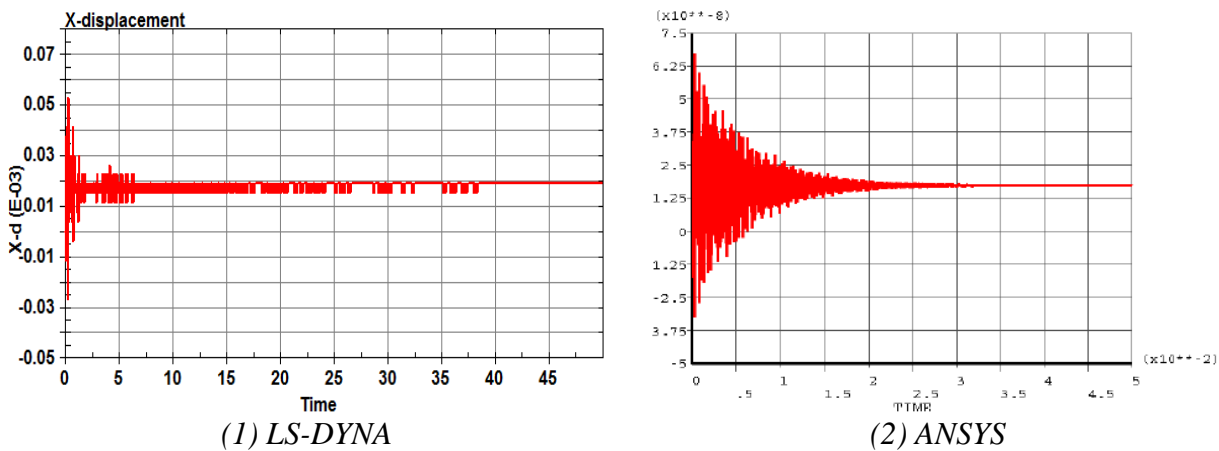
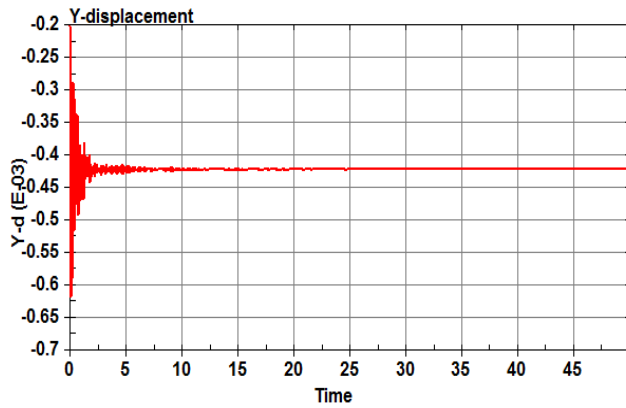
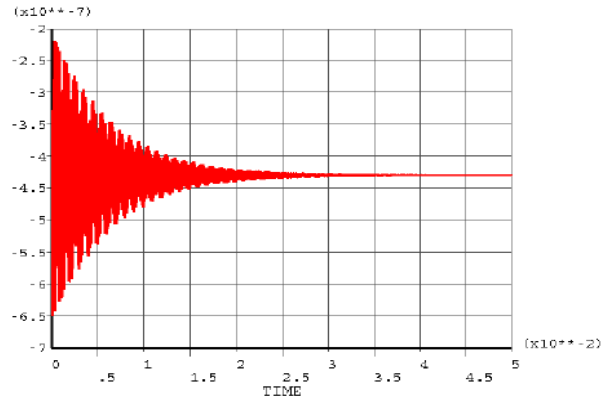


Figure 7 The x-displacement of node 11 for the model in Figure 6

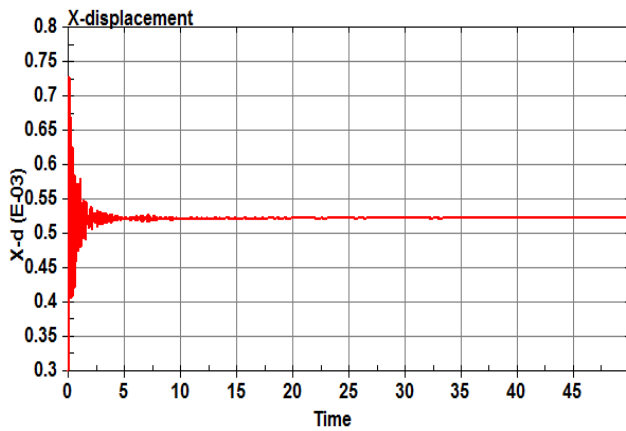


(1) LS-DYNA

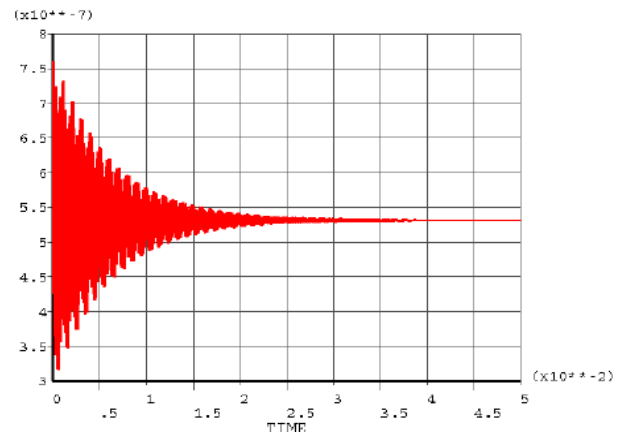


(2) ANSYS

Figure 8 The y-displacement of node 11 for the model in Figure 6

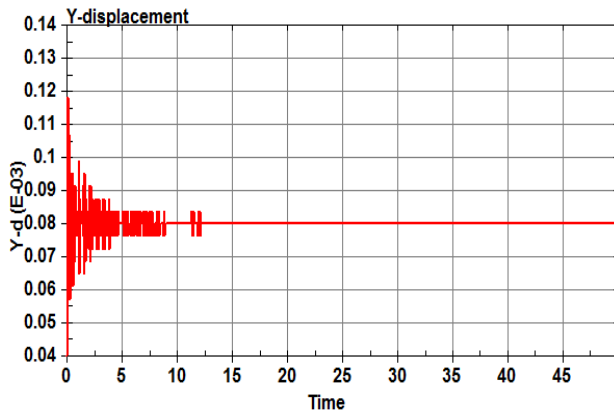


(1) LS-DYNA

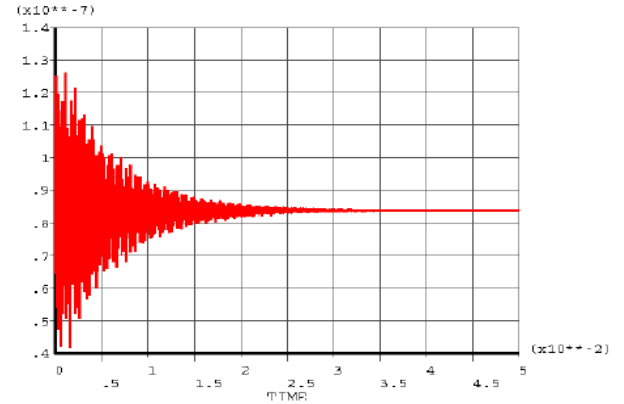


(2) ANSYS

Figure 9 The x-displacement of node 143 for the model in Figure 6



(1) LS-DYNA



(2) ANSYS

Figure 10 The y-displacement of node 143 for the model in Figure 6

3.2 Shaft whirling orbit

The shaft model is the same as the one shown in Figure 1. The x-displacement of the shaft center obtained from LS-DYNA and ANSYS when the shaft is rotating at a speed of 200 rad/s are plotted in Figure 11. Although the displacements are not exactly the same for the two simulations, the averaged values are very close ($3e-3$ m) and the response frequencies are almost the same. The shaft center whirling orbits are shown in Figure 12 (x-axis is the x displacement and y-axis is the y displacement). It shows that the whirling center ($3e-3$ m, 0 m) is very close for the two simulations. Moreover, the shaft movements are very similar. We also present the shaft center state-spaces (displacement vs. velocity) in the x-axis direction in Figure 13. Again, it indicates that the movements of the shaft are almost the same.

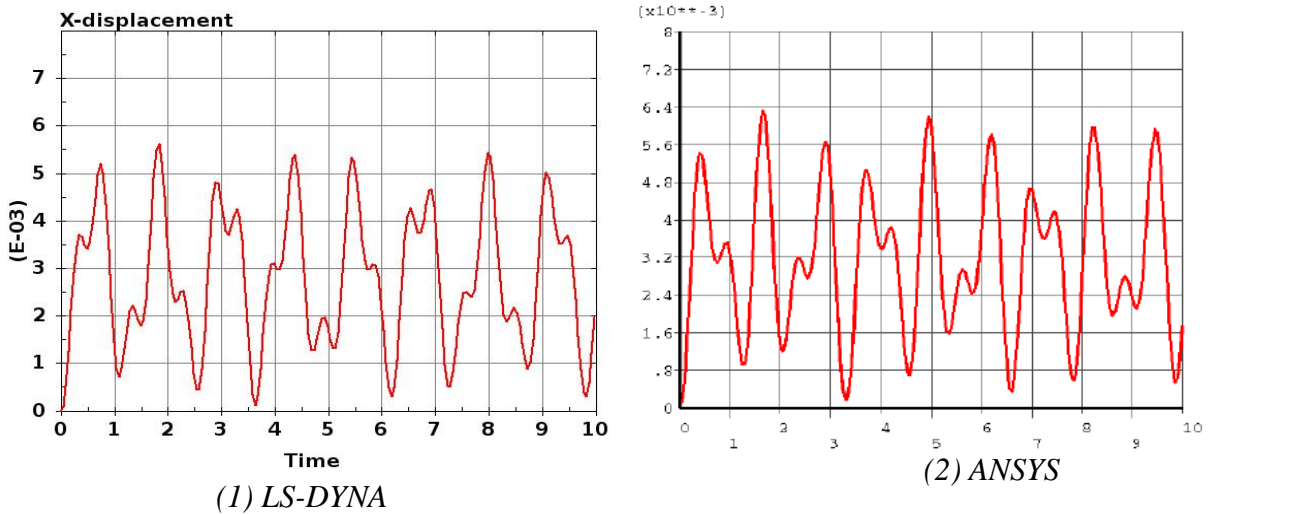


Figure 11 The x-displacement of the shaft center

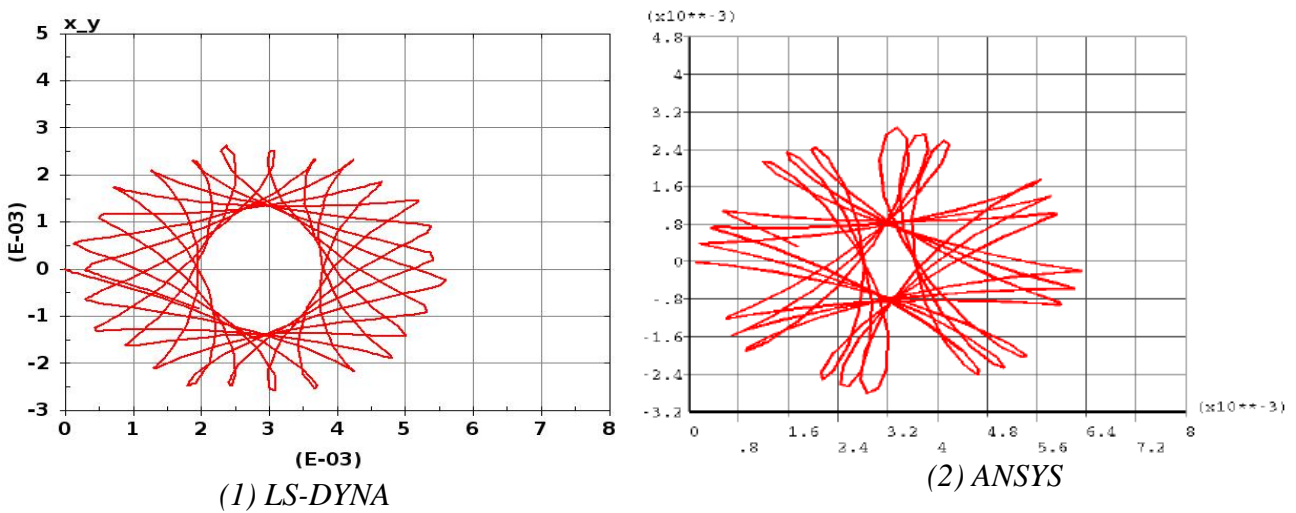
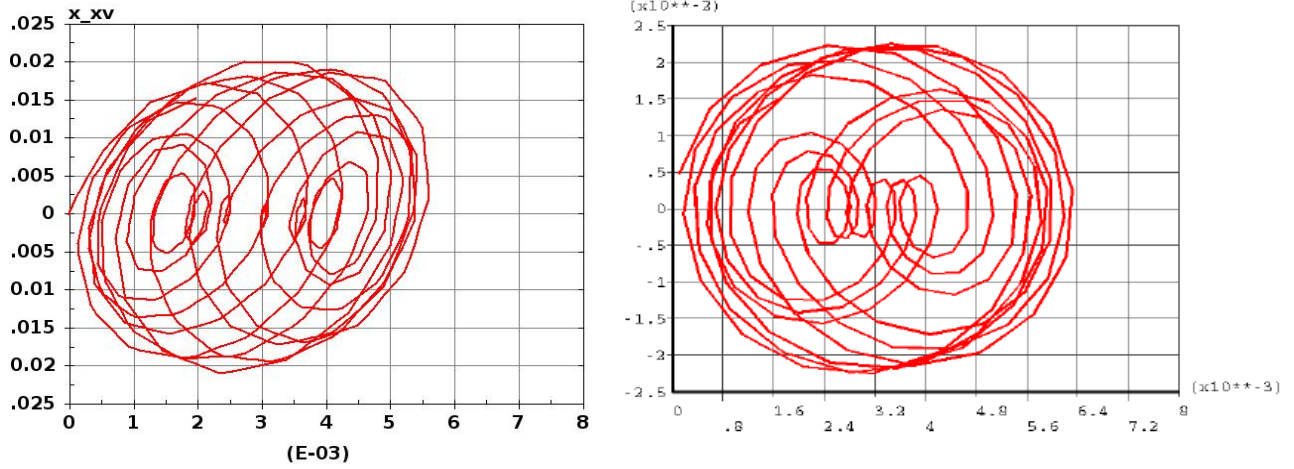


Figure 12 The shaft center whirling orbit



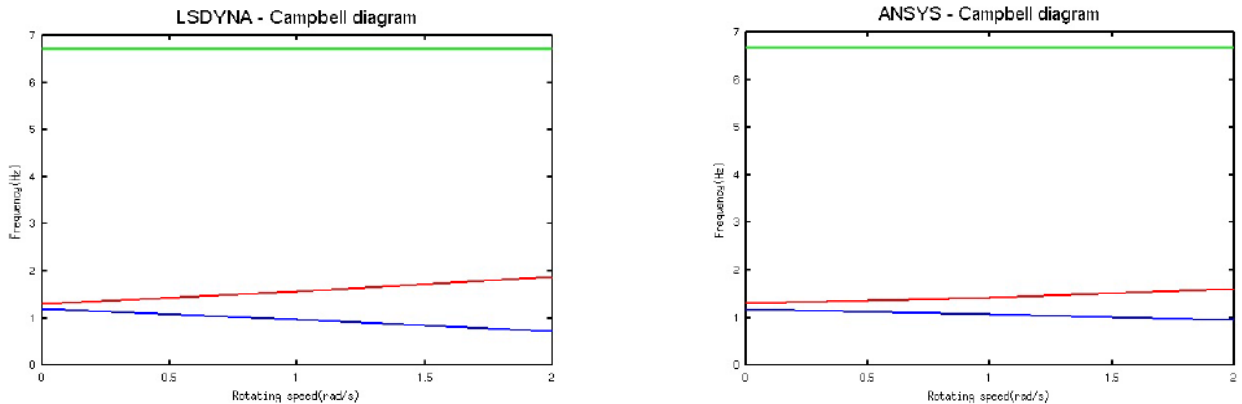
(1) LS-DYNA

(2) ANSYS

Figure 13 The shaft center state-space (displacement vs. velocity)

3.3 Campbell Diagram

In rotor dynamical system, the mode frequencies often depend on the rotating speeds due to the gyroscopic damping and softening stiffness effects. In order to test LS-DYNA’s capability to simulate the system’s response spectrum, we plotted the Campbell diagrams of a shaft and a disk model and they are compared with the ANSYS results. Figure 14 shows the Campbell diagrams of the first three modes for the shaft model in Figure 1 using the two software LS-DYNA and ANSYS. When the rotating speed is zero, the two simulations give almost the same mode frequencies. When the rotating speed increases, the first two mode frequencies begin to split and the change tendencies are the same for both LS-DYNA and ANSYS, while the third mode frequencies (green curve) don’t depend on the rotating speed for both simulations.



(1) LS-DYNA

(2) ANSYS

Figure 14 Campbell diagram for the shaft model

Figure 15 shows the Campbell diagrams of the first five mode frequencies for the disk model shown in Figure 16. The magnitudes of mode frequencies and the mode splitting phenomenon are almost the same using the two software. From the above two Campbell diagram analysis, we

can say that LS-DYNA can accurately capture the mode frequency changes with the change of rotating speed for the two cases in this section.

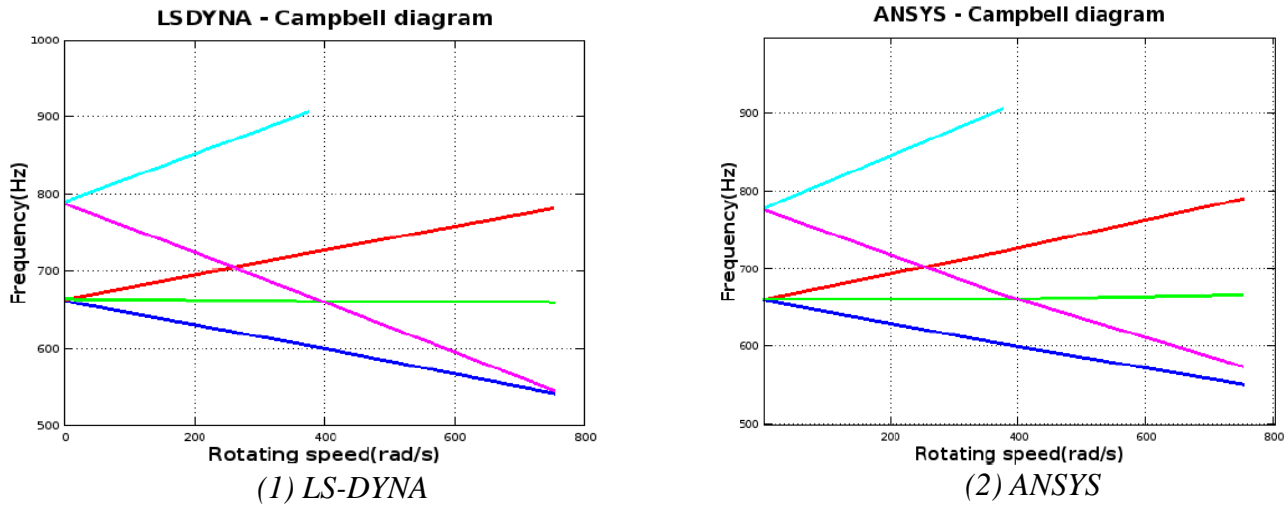


Figure 15 Campbell diagram for a disk model

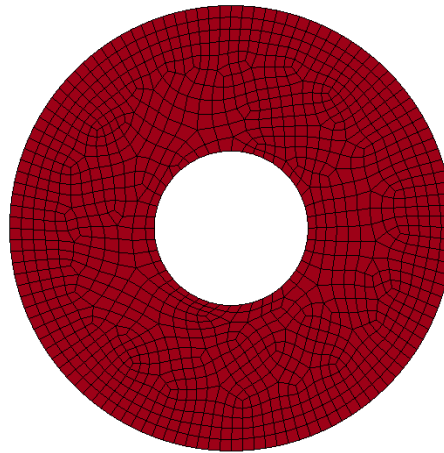


Figure 16 The disk model used in Figure 15

4. Conclusion

A new keyword card `*CONTROL_IMPLICIT_ROTATIONAL_DYNAMICS` is added to LS-DYNA to do rotor dynamics analysis. In order to test this new feature, the structural displacements due to rotating are verified using the theoretical results or simulation results from another finite element software ANSYS for the four different models with beam, shell and solid elements. The shaft whirling orbit and the Campbell diagram are also produced by this new implemented feature in LS-DYNA and the results are compared with ANSYS. All the analysis shows that LS-DYNA could give very similar results as theoretical results or ANSYS results, so we can say that the rotor dynamics analysis in LS-DYNA is accurate for the cases studied in this paper. However, there are still lots of studies needed to be done in the future for the rotor

dynamics analysis in LS-DYNA, such as modal analysis, resonant vibrations and etc. These are all under development.

5. References

[1] A.Vollan and L. Komzsik. (2012), Computational Techniques of Rotor Dynamics with the Finite Element Method, CRC Press.

[2] M. I. Friswell, J. E. T. Penny, S. D. Garvey and A. W. Lees. (2010), Dynamics of Rotating Machines, Cambridge University Press.

[3] J. Barlow. (1993), Finite Element Formulation of Flexible Rotor Whirling, Rolls-Royce plc, UK.

[4] R. Baddour and J. W. Zu. A revisit of spinning disk models. Part I: derivation of equations of motion. Applied Mathematical Modelling, 25(7):541~559, 2001a.